A comparison between a refined two-point model for the limited tokamak SOL and self-consistent plasma turbulence simulations

C. Wersal[1], P. Ricci[1], J. Loizu[2]

March 7, 2017

[1] Ecole Polytechnique Fédérale de Lausanne (EPFL), Swiss Plasma Center (SPC), CH-1015 Lausanne, Switzerland
[2] Max-Planck-Institut für Plasmaphysik, D-17491 Greifswald, Germany

Abstract
A refined two-point model is derived from the drift-reduced Braginskii equations for the limited tokamak scrape-off layer (SOL) by balancing the parallel and perpendicular transport of plasma and heat and taking into account the plasma-neutral interaction. The model estimates the electron temperature drop along a field line, from a region far from the limiter to the limiter plates. Self-consistent first-principles turbulence simulations of the SOL plasma including its interaction with neutral atoms are performed with the GBS code and compared to the refined two-point model. The refined two-point model is shown to be in very good agreement with the turbulence simulation results.

1 Introduction

The level of impurities in the core of a tokamak and the lifetime of the plasma facing components, two critical issues on the way to fusion energy, depend on the amount of sputtering of wall material [1]. Sputtering occurs when ions, accelerated in the sheath, hit the solid wall. The acceleration is directly related to the electron and ion temperature in front of the divertor or limiter

plates [2]. Therefore, understanding the physical processes that regulate the plasma temperature in front of the solid walls is of paramount importance.

Predictions of the conditions in front of the solid walls can be obtained by using three-dimensional simulations of the turbulent dynamics in the outermost plasma region of a fusion device, the scrape-off layer (SOL). A number of simulation codes were developed in the past years to carry out these simulations, such as BOUT++ [3], GBS [4, 5], GRILLIX [6], and TOKAM3X [7]. However, their development is still ongoing and turbulence simulations remain computationally very expensive. For this reason, progress was made in the development of simplified models that describe perpendicular turbulent transport as a diffusive process with diffusion coefficients obtained from fitting experimental data. Widely used transport codes that use these models are, e.g., SOLEDGE2D-EIRENE [8], SOLPS formerly B2-EIRENE [9, 10, 11], EMC3-EIRENE [12], and UEDGE [13]. Progress has been made to include the effect of turbulent fluctuations on neutral dynamics in these transport codes by adding stochastic fluctuations to plasma density and temperature, with characteristics similar to SOL turbulence [14]. Further simplifications of these transport models lead to the so-called two-point models [2], which are widely used to obtain fast, although rough, estimates of plasma parameters in front of the solid walls. Two-point models can be used to understand basic trends of the parallel transport in the tokamak SOL. They use assumptions about the perpendicular heat and particle fluxes and a one-dimensional description of the plasma dynamics along the field lines to obtain relations between the plasma parameters at the target (the divertor or limiter plates) and upstream (a location far from the target and in contact with the core, e.g., close to the X-point, where the divertor legs begin, or at the low-field side midplane). While a number of two-point models were developed in the past for different magnetic geometries, varying in their assumptions and inclusion of different physical processes (see, e.g., Refs. [15, 16, 17, 2]), to our knowledge no direct comparison of two-point models with the results of turbulence codes was carried out. The goal of the present paper is to perform such a comparison between fluid turbulent simulation results and two-point models in a rather low temperature regime ($T_\mathrm{e} \approx 3 - 15\mathrm{eV}$), and develop a two-point model that can well represent the simulation results. A two-point model that successfully predicts features of self-consistent turbulence simulations has the possibility to guide the decision about parameters of new simulations or even experiments, while reducing the number of computationally expensive turbulence simulations.

The comparison between two-point models and simulation results is performed by evaluating the electron temperature drop from the upstream to the target regions in a very simple magnetic configuration, i.e. a tokamak with circular magnetic flux surfaces and a toroidal rail limiter on the high-field side equatorial midplane. In this case, the targets are the lower and upper sides of the limiter, while the upstream location is at the low-field side equatorial midplane, halfway between the two targets. Since in the limited configuration the target location is next to the confined region, a large fraction of the recycled neutral atoms are ionized inside the last closed flux surface (LCFS), even in high density plasmas, where the ionization mean free path is short. The plasma can redistribute itself poloidally in the closed flux surface region, by moving along the magnetic field lines, and it flows back out to the SOL also at locations far from the limiter. Therefore, plasma parallel flows towards the limiter are important and, contrary to what is often done for high-density divertor configurations [2], the parallel convective heat flux cannot be neglected. Therefore, the simplest two-point model in limited configuration is derived from the balance between perpendicular heat transport, parallel heat conduction, and parallel heat convection (used as the basic model where plasma-neutral interactions are not important in [16], or as a starting point to derive the basic divertor two-point model in [2]). In the present paper, we compare the predictions of the simplest two-point model to first-principles turbulence simulations carried out with the GBS code. Since the comparison is not completely satisfactory, we derive a more refined two-point model rigorously from the fluid drift-reduced Braginskii equations, which are coupled to a kinetic equation for neutral atoms. The comparison of this refined model with the turbulence simulations shows very good agreement.

The present paper is structured as follows. After the Introduction, in Sec. 2 we describe a simple two-point model for toroidally limited tokamaks. Sec. 3 compares the prediction of this model with the SOL turbulence simulations. In Sec. 4 we develop a more accurate two-point model, which we compare to the turbulent simulations. A discussion and the conclusions follow in Sec. 5.

2 A simple two-point model for the limited SOL

In this Section we describe a simple two-point model for an axi-symmetric tokamak with a toroidal limiter. We consider one flux tube, which spans along a magnetic field line from one side to the other side of the limiter. We assume that the limiter is located at the high-field side equatorial midplane. We label the direction along the flux tube with the coordinate s, which spans from $s = -L$ at the lower side of the limiter, to $s = +L$ at its upper side, with the upstream location, $s = 0$, located at the low-field side equatorial midplane.

Since in the limited configuration the target location is next to the confined region, a large fraction of the recycled neutral atoms is ionized, even in high density plasmas, inside the closed flux surface region, where the ionized particles can redistribute poloidally before they flow back into the SOL. As a consequence, large plasma flows towards the limiter are present (even far from the limiter) and the parallel convective heat flux cannot be neglected. Therefore, the simplest two-point model in limited configuration is derived from the balance between the heat deposited in the flux tube due to the radial heat transport, $S_{Q\perp}$, the parallel heat conduction, Q_{cond}, and the parallel heat convection, Q_{conv}, i.e.

$$Q_{cond}(s) + Q_{conv}(s) = \int_0^s S_{Q\perp}(s')ds'. \tag{1}$$

In Eq. (1) we impose $Q_{cond}(0) = Q_{conv}(0) = 0$ because the upstream location, $s = 0$, is both a symmetry and a stagnation point in this simple model. The conductive heat flux is modeled by using the Spitzer heat flux coefficient, $Q_{cond} = -\chi_{e0} T_e^{5/2} dT_e/ds$, and the convective heat flux is estimated by taking the third-order moment of a shifted Maxwellian velocity distribution and neglecting the fluid kinetic energy contribution as $Q_{conv} = c_{e0}\Gamma T_e$, where $c_{e0} = 5/2$, and $\Gamma = \int S_{n\perp} ds$ is the parallel particle flux, with $S_{n\perp}$ being the particle source due to radial transport into the flux tube. Assuming $S_{Q\perp}$ and $S_{n\perp}$ constant along the flux tube in a limited geometry (corresponding to poloidally uniform outflow of plasma and heat), the equation that determines the electron temperature is

$$-\chi_{e0} T_e^{5/2} \frac{dT_e}{ds} + c_{e0} s S_{n\perp} T_e = s S_{Q\perp}. \tag{2}$$

The solution of Eq. (2) requires a boundary condition that we apply at the magnetic pre-sheath entrance by writing the electron heat flux through the sheath entrance as $Q_t = \gamma_e \Gamma_t T_{e,t}$, where the subscript t indicates the target location, which is the magnetic pre-sheath entrance, and the coefficient $\gamma_e \approx 5$ is the electron sheath transmission coefficient [2].

Equation (2) can be integrated numerically for a given $S_{Q\perp}$ and $S_{n\perp}$ by imposing the sheath boundary condition. An implicit analytical expression to relate the electron temperature at the target, $T_{e,t}$, to its upstream value, $T_{e,u}$, can also be obtained [16] and evaluated numerically.

The simplest two-point model we describe here, Eq. (2), is often used in the literature, e.g. as a starting point to derive the simple divertor two-point model in [2] or as a basic model in regions where plasma-neutral interactions are not important in [16].

3 Turbulent SOL simulations and comparison with the simple two-point model

In this Section we introduce the model that we use to describe plasma turbulence in the tokamak SOL and its interaction with neutrals, by outlining the basic assumptions of the model and presenting the resulting equations. (A more complete derivation can be found in Refs. [18, 19].) The electron temperature drop from the upstream to the target location predicted by this model, which is implemented in the GBS code [4, 5], is then compared with the simple two-point model.

Since the plasma in the SOL is rather cold (compared to the core), its collisionality is often sufficiently high that a fluid model, such as Braginskii's model [20], can be used for its description. Moreover, by taking advantage of the fact that plasma turbulence is elongated along the field lines ($k_\parallel \ll k_\perp$) and that turbulent timescales are much slower than the ion cyclotron motion ($\partial/\partial t \ll \Omega_{ci}$), the drift reduction can be applied [18]. This leads, together with quasi-neutrality, to a set of drift-reduced two-fluid Braginskii equations that describe the dynamics of plasma density, n, generalized vorticity, $\tilde{\omega}$, electron and ion parallel velocities, $v_{\parallel \mathrm{e}}$ and $v_{\parallel \mathrm{i}}$, and electron and ion temperatures, T_e and T_i. In the electrostatic limit these equations are

$$\frac{\partial n}{\partial t} = -\frac{1}{B}[\phi, n] - \nabla_\parallel (n v_{\parallel \mathrm{e}}) + \frac{2}{eB}\left[C(p_\mathrm{e}) - enC(\phi)\right] + \mathcal{D}_n(n) + S_n \tag{3}$$
$$+ n_\mathrm{n}\nu_\mathrm{iz} - n\nu_\mathrm{rec}$$
$$\frac{\partial \tilde{\omega}}{\partial t} = -\frac{1}{B}[\phi, \tilde{\omega}] - v_{\parallel \mathrm{i}}\nabla_\parallel \tilde{\omega} + \frac{B^2}{m_\mathrm{i} n}\nabla_\parallel j_\parallel + \frac{2B}{m_\mathrm{i} n}C(p) + \mathcal{D}_{\tilde{\omega}}(\tilde{\omega}) - \frac{n_\mathrm{n}}{n}\nu_\mathrm{cx}\tilde{\omega} \tag{4}$$
$$\frac{\partial v_{\parallel \mathrm{e}}}{\partial t} = -\frac{1}{B}[\phi, v_{\parallel \mathrm{e}}] - v_{\parallel \mathrm{e}}\nabla_\parallel v_{\parallel \mathrm{e}} + \frac{e}{\sigma_\parallel m_\mathrm{e}} j_\parallel \tag{5}$$
$$+ \frac{e}{m_\mathrm{e}}\nabla_\parallel \phi - \frac{T_\mathrm{e}}{m_\mathrm{e} n}\nabla_\parallel n - \frac{1.71}{m_\mathrm{e}}\nabla_\parallel T_\mathrm{e} + \mathcal{D}_{v_{\parallel \mathrm{e}}}(v_{\parallel \mathrm{e}})$$
$$+ \frac{n_\mathrm{n}}{n}(\nu_\mathrm{en} + 2\nu_\mathrm{iz})(v_{\parallel \mathrm{n}} - v_{\parallel \mathrm{e}})$$
$$\frac{\partial v_{\parallel \mathrm{i}}}{\partial t} = -\frac{1}{B}[\phi, v_{\parallel \mathrm{i}}] - v_{\parallel \mathrm{i}}\nabla_\parallel v_{\parallel \mathrm{i}} - \frac{1}{m_\mathrm{i} n}\nabla_\parallel p + \mathcal{D}_{v_{\parallel \mathrm{i}}}(v_{\parallel \mathrm{i}}) \tag{6}$$
$$+ \frac{n_\mathrm{n}}{n}(\nu_\mathrm{iz} + \nu_\mathrm{cx})(v_{\parallel \mathrm{n}} - v_{\parallel \mathrm{i}})$$
$$\frac{\partial T_\mathrm{e}}{\partial t} = -\frac{1}{B}[\phi, T_\mathrm{e}] - v_{\parallel \mathrm{e}}\nabla_\parallel T_\mathrm{e} + \frac{4T_\mathrm{e}}{3eB}\left[\frac{T_\mathrm{e}}{n}C(n) + \frac{7}{2}C(T_\mathrm{e}) - eC(\phi)\right] \tag{7}$$
$$+ \frac{2T_\mathrm{e}}{3n}\left[\frac{0.71}{e}\nabla_\parallel j_\parallel - n\nabla_\parallel v_{\parallel \mathrm{e}}\right] + \mathcal{D}_{T_\mathrm{e}}(T_\mathrm{e}) + \kappa_{\parallel \mathrm{e}}\nabla_\parallel (T_\mathrm{e}^{5/2}\nabla_\parallel T_\mathrm{e}) + S_{T_\mathrm{e}}$$
$$+ \frac{n_\mathrm{n}}{n}\nu_\mathrm{iz}\left[-\frac{2}{3}E_\mathrm{iz} - T_\mathrm{e} + m_\mathrm{e} v_{\parallel \mathrm{e}}\left(v_{\parallel \mathrm{e}} - \frac{4}{3}v_{\parallel \mathrm{n}}\right)\right] - \frac{n_\mathrm{n}}{n}\nu_\mathrm{en} m_\mathrm{e}\frac{2}{3}v_{\parallel \mathrm{e}}(v_{\parallel \mathrm{n}} - v_{\parallel \mathrm{e}})$$
$$\frac{\partial T_\mathrm{i}}{\partial t} = -\frac{1}{B}[\phi, T_\mathrm{i}] - v_{\parallel \mathrm{i}}\nabla_\parallel T_\mathrm{i} + \frac{4T_\mathrm{i}}{3eB}\left[C(T_\mathrm{e}) + \frac{T_\mathrm{e}}{n}C(n) - \frac{5}{2}C(T_\mathrm{i}) - eC(\phi)\right] \tag{8}$$
$$+ \frac{2T_\mathrm{i}}{3n}\left[\frac{1}{e}\nabla_\parallel j_\parallel - n\nabla_\parallel v_{\parallel \mathrm{i}}\right] + \mathcal{D}_{T_\mathrm{i}}(T_\mathrm{i}) + \kappa_{\parallel \mathrm{i}}\nabla_\parallel (T_\mathrm{i}^{5/2}\nabla_\parallel T_\mathrm{i}) + S_{T_\mathrm{i}}$$
$$+ \frac{n_\mathrm{n}}{n}(\nu_\mathrm{iz} + \nu_\mathrm{cx})\left[T_\mathrm{n} - T_\mathrm{i} + \frac{1}{3}(v_{\parallel \mathrm{n}} - v_{\parallel \mathrm{i}})^2\right]$$

with $p = n(T_\mathrm{e} + T_\mathrm{i})$ the total pressure, $j_\parallel = en(v_{\parallel \mathrm{i}} - v_{\parallel \mathrm{e}})$ the parallel current, $\kappa_{\parallel \mathrm{e}}$ and $\kappa_{\parallel \mathrm{i}}$ the Spitzer heat conduction coefficients, E_iz the effective ionization energy, and $\sigma_\parallel = 1.96e^2 n\tau_\mathrm{e}/m_\mathrm{e}$, the parallel conductivity, where τ_e is the electron collision time. The generalized vorticity, $\tilde{\omega} = \omega + 1/e\nabla_\perp^2 T_\mathrm{i}$, is related to the electrostatic potential by $\nabla_\perp^2 \phi = \omega$. The following operators are used

$\nabla_\parallel A = \hat{\mathbf{b}}\cdot\nabla A$, $[A_1, A_2] = \hat{\mathbf{b}}\cdot(\nabla A_1 \times \nabla A_2)$, and $C(A) = B/2[\nabla\times(\hat{\mathbf{b}}/B)]\cdot\nabla A$ with $\hat{\mathbf{b}} = \mathbf{B}/B$. The source terms ($S_n$, S_{T_e}, S_{T_i}) mimic the outflow of hot plasma from the confined region to the SOL, and we interpret their location as the radial position of the LCFS. The perpendicular diffusive terms $\mathcal{D}_A(A)$ are included mostly for numerical reasons. The system is closed by a set of first-principles boundary conditions applied at the magnetic pre-sheath entrance of the limiter plates, derived and discussed in Ref. [21].

The interaction of the plasma with the neutral atoms, rigorously deduced from a kinetic description [19], is included through the interaction with the neutral density, n_n, parallel velocity, $v_{\parallel\mathrm{n}}$, and temperature, T_n. These moments of the neutral distribution function are obtained from the solution of the kinetic neutral equation for a mono-atomic neutral species

$$\frac{\partial f_\mathrm{n}}{\partial t} + \mathbf{v}\cdot\frac{\partial f_\mathrm{n}}{\partial \mathbf{x}} = -\nu_\mathrm{iz} f_\mathrm{n} - \nu_\mathrm{cx}\left(f_\mathrm{n} - \frac{n_\mathrm{n}}{n_\mathrm{i}} f_\mathrm{i}\right) + \nu_\mathrm{rec} f_\mathrm{i} \tag{9}$$

where f_n and f_i are the neutral and ion distribution functions. The ionization, charge-exchange, and recombination processes as well as the elastic electron-neutral collisions are described, respectively, through the use of Krook operators with collision frequencies defined as $\nu_\mathrm{iz} = n_\mathrm{e}\langle v_\mathrm{e}\sigma_\mathrm{iz}(v_\mathrm{e})\rangle$, $\nu_\mathrm{rec} = n_\mathrm{e}\langle v_\mathrm{e}\sigma_\mathrm{rec}(v_\mathrm{e})\rangle$, $\nu_\mathrm{cx} = n_\mathrm{i}\langle v_\mathrm{i}\sigma_\mathrm{cx}(v_\mathrm{i})\rangle$, and $\nu_\mathrm{en} = n_\mathrm{e}\langle v_\mathrm{e}\sigma_\mathrm{en}(v_\mathrm{e})\rangle$, where σ_iz, σ_rec, σ_cx, and σ_en are the ionization, recombination, charge-exchange, and elastic electron-neutral cross sections. (The $\langle\cdot\rangle$ operator denotes the averaging over the Maxwellian electron, or ion, distribution function. We note that we neglected the electron-neutral collisions in Eq. (9) due to the high electron to neutral mass ratio [19].) This neutral model has been chosen to be as simple as possible, while still keeping the main plasma-neutral interactions with a kinetic neutral description to allow for short and long neutral mean free path simulations. Although molecular processes become important at low temperatures, especially for quantitative comparison with experiments, they are neglected in the current model to facilitate the interpretation and understanding of the plasma-neutral interaction in the turbulent SOL.

Eqs. (3-8) are solved by the GBS code using a second order finite difference scheme, except for the $[A_1, A_2]$ operators that are discretized by using the Arakawa scheme [22]. Time integration is carried out with the classical Runge-Kutta method [23]. The solution of Eq. (9) is obtained in the limit of $\tau_\mathrm{n} < \tau_\mathrm{turb}$ (τ_n is the mean flight time of a neutral atom, τ_turb is the turbulent timescale) and $1/k_\parallel > \lambda_\mathrm{mfp}$ (λ_mfp is the mean free path of the neutrals) by using the method of characteristics [19].

To compare the simple two-point model with results from the GBS code, we consider six simulations, with a toroidal limiter on the high-field equatorial midplane, $R = 500\rho_{s0}$, R being the major radius, $m_i/m_e = 400$, $2\pi a = 800\rho_{s0}$, a being the minor radius, $\rho_{s0} = c_{s0}/\Omega_{ci}$, $\Omega_{ci} = eB_0/m_i$, $c_{s0} = \sqrt{T_{e0}/m_i}$. With $T_{e0} = T_{i0} = 10$eV and $B_0 = 0.5$T, it results $R \simeq 31$cm and $a \simeq 8$cm. (We note that with $T_{e0} = 10$eV we can neglect the recombination processes, since $\nu_{rec}/\nu_{iz} \approx 10^{-5}$. In our simple atomic neutral model this assumption holds for $T_e \gtrsim 2$eV, corresponding to $\nu_{rec}/\nu_{iz} \lesssim 10^{-2}$.) The six simulations are variants of two basic configurations, characterized by two different plasma densities, which were also used in Ref. [19]. In the low plasma density configuration, we impose $n_0 = 5 \cdot 10^{18}\mathrm{m}^{-3}$, the value of the density at the LCFS. As a consequence, the resistivity normalized to R/c_{s0} is $\tilde{\nu} = Rm_e/(1.96c_{s0}m_i\tau_e) = 0.02$, the dimensionless parallel electron heat conductivity is $\tilde{\kappa}_{\parallel e} = 3.16 \times 2T_{e0}\tau_e/(3m_e c_{s0}R) = 56.0$, and the dimensionless parallel ion heat conductivity is $\tilde{\kappa}_{\parallel i} = 3.9 \times 2T_{i0}\tau_i/(3m_i c_{s0}R) = 1.6$. In the high plasma density configuration, $n_0 = 5 \cdot 10^{19}\mathrm{m}^{-3}$, $\tilde{\nu} = 0.2$, $\tilde{\kappa}_{\parallel e} = 5.6$, and $\tilde{\kappa}_{\parallel i} = 0.16$ are used. In addition to these two basic simulations, we repeat both simulations zeroing out the plasma interaction terms with the neutral atoms. These simulations are labeled as 'no n_n' in the following. For the high density case, we also carry out a simulation where we change the energy removed by each ionization to include the increased energy loss due to multiple impact ionizations, labeled as '$E_{iz} = 30$eV' (in the other cases $E_{iz} = 13.6$eV) and a simulation labeled 'high S_T', where we increase the temperature sources S_{T_e} and S_{T_i} by a factor of four and the density source S_n by 30%, which results in twice the temperature and about the same density as in the basic high density simulation. (The electron temperature increases at the target from 3.8eV to 7.2eV and at the low-field side midplane from 6.4eV to 13.8eV in the closest flux-tube to the core, centered around $r - r_{LCFS} = 15\rho_{s0}$.) The computational domain extends for all six simulations from $r_{min} = 0$ to $r_{max} = 150\rho_{s0}$. The source terms S_n, S_{T_i}, and S_{T_e} in Eqs. (3-8) are constant in time, poloidally uniform, and radially Gaussian around $r_s = 30\rho_{s0}$ with a width of $5\rho_{s0}$.

The comparison with the simple two-point model is performed for five different flux tubes extending radially over $10\rho_{s0}$ centered at $r - r_{LCFS} = 15, 25, 35, 45, 55\rho_{s0}$. To calculate the particle and heat deposited into each flux tube, $S_{n\perp}$ and $S_{Q\perp}$, we combine the perpendicular drift terms in the GBS equations (as explained in Sec. 4), and we average them over time and over the poloidal direction.

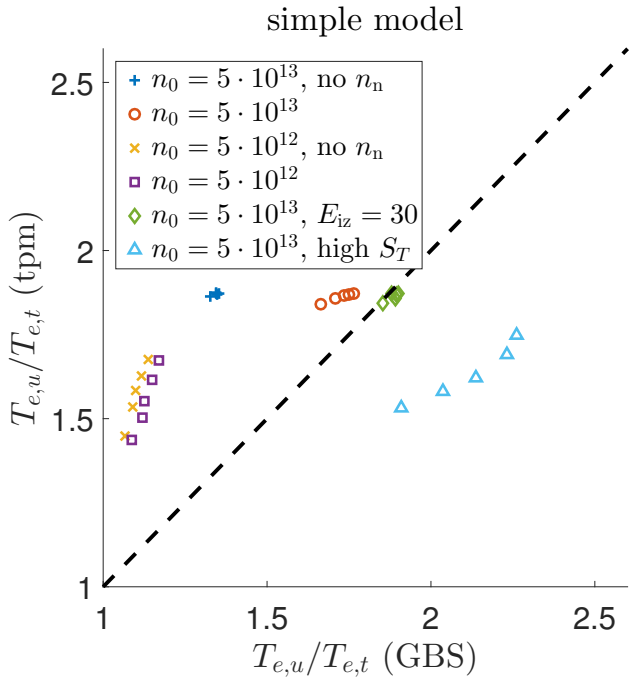

Figure 1: Comparison of the ratio between the electron temperature at the upstream and target locations, $T_{\mathrm{e,u}}/T_{\mathrm{e,t}}$, predicted by the simple two-point model, Eq. (2), (tpm), with the results of a set of GBS simulations. For each simulation (different colors) we consider five flux tubes of width $10\rho_{\mathrm{s0}}$ centered at radial locations $r - r_{\mathrm{LCFS}} = 15, 25, 35, 45, 55\rho_{\mathrm{s0}}$.

The two-point model estimates of the temperature ratio, $T_{\mathrm{e,u}}/T_{\mathrm{e,t}}$, are then compared to the temperature ratio in the simulations. The results are shown in Fig. 1. While the general trend for the different radial locations in each simulation is captured by the simple two-point model, the agreement with the turbulent simulations shows relative errors that are up to 50% for this set of simulations.

4 A refined two-point model for limited SOL

In this Section, we derive a refined two-point model rigorously from the drift-reduced Braginskii equations for plasma density, Eq. (3), and electron temperature, Eq. (7). The perpendicular diffusive terms, $\mathcal{D}_n(n)$ and $\mathcal{D}_{T_{\mathrm{e}}}(T_{\mathrm{e}})$, included mostly for numerical reasons, can be neglected, since they are small.

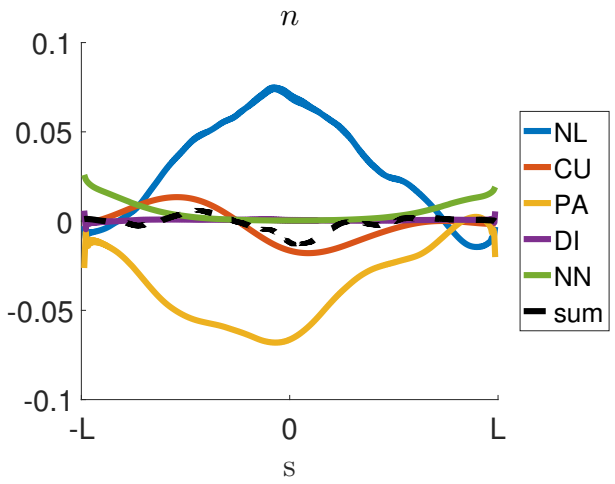

Figure 2: Time-averaged plasma density balance along the field lines between the two limiter plates for the high density simulation for a flux tube with a width of $10\rho_{s0}$ centered at $r - r_{\mathrm{LCFS}} = 25\rho_{s0}$. The contributions are NL $= -[\phi, n]/B$ ($\mathbf{E}\times\mathbf{B}$ advection), CU $= 2[C(p_e) - enC(\phi)]/eB$ (divergence of diamagnetic and $\mathbf{E}\times\mathbf{B}$ flow due to curvature), PA $= -\nabla_\parallel(nv_{\parallel e})$ (parallel advection), DI $= \mathcal{D}_n(n)$ (perpendicular diffusion), and NN $= n_n\nu_{iz}$ (plasma-neutral interaction term). The sum in black shows the quasi steady state balance is almost exact. It does not vanish perfectly because of the finite time-average and the finite sampling rate of the simulation results.

For typical parameters of limited tokamaks, the SOL plasma temperature is sufficiently high to neglect recombination processes. Furthermore, we neglect the terms in the electron temperature equation, Eq. (7), associated with the difference between parallel electron and neutral velocities since they are small compared to the other plasma-neutral interaction terms. We also assume $j_\parallel = 0$ in Eq. (7). The validity of these assumptions is shown in Figs. 2 and 3. By making use of these assumptions, we obtain

$$\frac{\partial n}{\partial t} + \nabla_\parallel(nv_{\parallel e}) = \tilde{S}_{n\perp} + \tilde{S}_{n,n_n} \tag{10}$$

$$\frac{\partial T_e}{\partial t} + v_{\parallel e}\nabla_\parallel T_e + \frac{2T_e}{3}\nabla_\parallel v_{\parallel e} - \kappa_e\nabla_\parallel(T_e^{5/2}\nabla_\parallel T_e) = \tilde{S}_{T_e\perp} + \tilde{S}_{T_e,n_n} \tag{11}$$

where we combine the perpendicular transport terms (the terms related to the $\mathbf{E}\times\mathbf{B}$ and diamagnetic drifts as well as the S_n and S_{T_e} terms) into

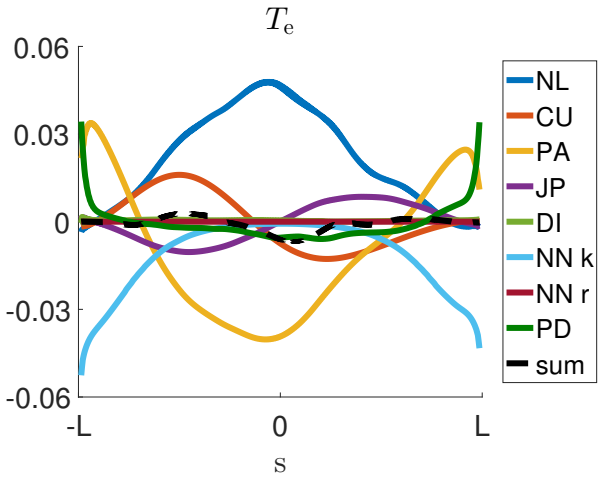

Figure 3: Time-averaged electron temperature balance for the same case as in Fig. 2. The contributions are NL $= -[\phi, T_\mathrm{e}]/B$ ($\mathbf{E}\times\mathbf{B}$ advection), CU $= 4T_\mathrm{e}[T_\mathrm{e}C(n)/n + 7C(T_\mathrm{e})/2 - eC(\phi)]/3eB$ (curvature), PA $= -v_{\parallel\mathrm{e}}\nabla_\parallel T_\mathrm{e} + 2T_\mathrm{e}\nabla_\parallel v_{\parallel\mathrm{e}}/3$ (parallel advection), JP $= 0.47T_\mathrm{e}\nabla_\parallel j_\parallel/en$ (parallel current term), DI $= \mathcal{D}_{T_\mathrm{e}}(T_\mathrm{e})$ (perpendicular diffusion), $\mathrm{NN_k} = n_\mathrm{n}\nu_\mathrm{iz}(-2E_\mathrm{iz}/3 - T_\mathrm{e})/n$ (plasma-neutral interaction terms that we keep in the analysis), $\mathrm{NN_r} = n_\mathrm{n}\nu_\mathrm{iz}m_\mathrm{e}v_{\parallel\mathrm{e}}(v_{\parallel\mathrm{e}} - 4v_{\parallel\mathrm{n}}/3)/n - n_\mathrm{n}\nu_\mathrm{en}m_\mathrm{e}2v_{\parallel\mathrm{e}}(v_{\parallel\mathrm{n}} - v_{\parallel\mathrm{e}})/3n$ (plasma-neutral interaction terms that we neglect), and PD $= \kappa_{\parallel\mathrm{e}}\nabla_\parallel(T_\mathrm{e}^{5/2}\nabla_\parallel T_\mathrm{e})$ (parallel conduction). The sum in black shows the quasi steady state balance is almost exact. It does not vanish perfectly because of the finite time-average and the finite sampling rate of the simulation results.

effective perpendicular source terms,

$$\tilde{S}_{n\perp} = -\frac{1}{B}[\phi, n] + \frac{2}{eB}\left[C(p_\mathrm{e}) - enC(\phi)\right] + S_n \tag{12}$$

$$\tilde{S}_{T_\mathrm{e}\perp} = -\frac{1}{B}[\phi, T_\mathrm{e}] + \frac{4T_\mathrm{e}}{3eB}\left[\frac{T_\mathrm{e}}{n}C(n) + \frac{7}{2}C(T_\mathrm{e}) - eC(\phi)\right] + S_{T_\mathrm{e}}, \tag{13}$$

and we do the same for the plasma-neutral interaction terms:

$$\tilde{S}_{n,n_\mathrm{n}} = n_\mathrm{n}\nu_\mathrm{iz} \tag{14}$$

$$\tilde{S}_{T_\mathrm{e},n_\mathrm{n}} = \frac{n_\mathrm{n}}{n}\nu_\mathrm{iz}\left(-\frac{2}{3}E_\mathrm{iz} - T_\mathrm{e}\right). \tag{15}$$

To obtain an equation for the parallel electron heat flux, we multiply Eq. (10) by $3T_e/2$, and Eq. (11) by $3n/2$ and we sum the two resulting

equations:

$$\frac{3}{2}\frac{\partial(nT_\mathrm{e})}{\partial t}+\frac{3}{2}T_\mathrm{e}\nabla_\parallel(nv_{\parallel\mathrm{e}})+\frac{3}{2}nv_{\parallel\mathrm{e}}\nabla_\parallel T_\mathrm{e}+nT_\mathrm{e}\nabla_\parallel v_{\parallel\mathrm{e}}-\frac{3}{2}n\kappa_\mathrm{e}\nabla_\parallel(T_\mathrm{e}^{5/2}\nabla_\parallel T_\mathrm{e}) \\ =\frac{3}{2}T_\mathrm{e}\tilde{S}_{n\perp}+\frac{3}{2}n\tilde{S}_{T_\mathrm{e}\perp}+\frac{3}{2}T_\mathrm{e}\tilde{S}_{n,n_\mathrm{n}}+\frac{3}{2}n\tilde{S}_{T_\mathrm{e},n_\mathrm{n}}. \tag{16}$$

We now time-average Eqs. (10) and (16) and, rearranging the terms, we obtain

$$\nabla_\parallel\left(nv_{\parallel\mathrm{e}}\right)\approx S_{n\perp}+S_{n,n_\mathrm{n}} \tag{17}$$

$$\nabla_\parallel\left(\frac{5}{2}nv_{\parallel\mathrm{e}}T_\mathrm{e}\right)-v_{\parallel\mathrm{e}}\nabla_\parallel\left(nT_\mathrm{e}\right)-\chi_\mathrm{e}\nabla_\parallel\left(T_\mathrm{e}^{5/2}\nabla_\parallel T_\mathrm{e}\right)\approx S_{Q\perp}-S_{n,n_\mathrm{n}}E_\mathrm{iz}, \tag{18}$$

with $S_{n\perp}$ and $S_{Q\perp}$ being the time average of $\tilde{S}_{n\perp}$ and $3/2(T_\mathrm{e}\tilde{S}_{n\perp}+n\tilde{S}_{T_\mathrm{e}\perp})$ respectively, and all quantities appearing in Eqs. (17-18) being time averaged. We note that, in agreement with simulation results, the contribution due to the correlation between fluctuations can be neglected when time-averaging the parallel transport terms and the neutral-plasma interaction terms (i.e., the terms that are the product of two or more fluctuating quantities can be evaluated as the product of the time-averaged multiplicands). On the other hand, the fluctuations have to be included in the time-averaging of the perpendicular turbulent transport terms to obtain $S_{n\perp}$ and $S_{Q\perp}$. Moreover, the coefficient in the parallel Spitzer heat conductivity is defined as $\chi_\mathrm{e}=\frac{3}{2}n_\mathrm{ft}\kappa_\mathrm{e}$, where n_ft is the average density in the flux tube.

To derive the electron temperature drop along the field lines from Eq. (18), we estimate the variation of the parallel electron velocity, plasma density, and neutral density along the field line. We assume that the parallel velocity varies linearly between the two limiters, where Bohm boundary conditions are valid, i.e.

$$v_{\parallel\mathrm{e}}(\pm L)=\pm c_\mathrm{s}=\pm\sqrt{\frac{T_\mathrm{e}+T_\mathrm{i}}{m_\mathrm{i}}}\approx\pm\sqrt{\frac{2T_\mathrm{e}}{m_\mathrm{i}}}, \tag{19}$$

obtaining therefore

$$v_{\parallel\mathrm{e}}(s)=\frac{c_s s}{L}. \tag{20}$$

To estimate the density profile, we integrate Eq. (17), that is

$$\Gamma = nv_{\parallel \mathrm{e}} = \int S_{n\perp} + S_{n,n_\mathrm{n}} ds. \tag{21}$$

The profile of the plasma density is then $n = \Gamma / v_{\parallel \mathrm{e}}$. The neutral density is assumed to decay exponentially from the two limiters, i.e.

$$n_n(s) = n_n(-L) \exp\left[(-s-L)/\lambda_{\mathrm{mfp}}\right] + n_n(L) \exp\left[(s-L)/\lambda_{\mathrm{mfp}}\right], \tag{22}$$

with the decaying scale length given by $\lambda_{\mathrm{mfp}} = \alpha_r c_s / (\nu_{\mathrm{iz}} + \nu_{\mathrm{cx}})$, where α_r is the reflection coefficient of the neutrals on the limiter [19] (the velocity of the thermal neutrals from the wall is much smaller and can be neglected when estimating the effective neutral mean free path). The collision frequencies ν_{iz} and ν_{cx} are evaluated with the electron temperature and plasma density averaged around the target (from the limiter to a distance λ_{mfp} from the limiter). The target density, $n_n(\pm L)$, is chosen to match the total amount of ionization in the considered flux tube. This is an input for an one-dimensional model, since neutral particles are not bound to flow along a field line and can move easily across the flux surfaces before being ionized. The ionization inside each flux tube amounts for about 5% to 20% of the recycled particles at its ends, depending mainly on plasma density and radial location of the considered flux tube. The perpendicular source terms, $S_{n\perp}$ and $S_{Q\perp}$, are approximated to have a cosine distribution due to the ballooning character of the perpendicular transport, which is confirmed by the turbulence simulations.

Finally, to solve (18) for the electron temperature, we impose symmetry around the upstream location $s = 0$, where the parallel derivative of T_e vanishes. We also ensure that the velocity profile is self-consistently evaluated with $T_e(\pm L)$ by enforcing that the integral of the parallel electron heat equation, Eq. (18), along s is satisfied, i.e.

$$\begin{aligned} \left[\frac{5}{2} n v_{\parallel \mathrm{e}} T_\mathrm{e}\right]_{-L}^{L} &= 5L\Gamma(\pm L) T_\mathrm{e}(\pm L) \\ &= \int_{-L}^{L} \left[S_{Q\perp} - S_{n,n_\mathrm{n}} E_{\mathrm{iz}} + v_{\parallel \mathrm{e}} \nabla_\parallel (n T_\mathrm{e}) + \chi_\mathrm{e} \nabla_\parallel (T_\mathrm{e}^{5/2} \nabla_\parallel T_\mathrm{e}) \right] ds, \end{aligned} \tag{23}$$

which describes the total heat balance in the flux tube.

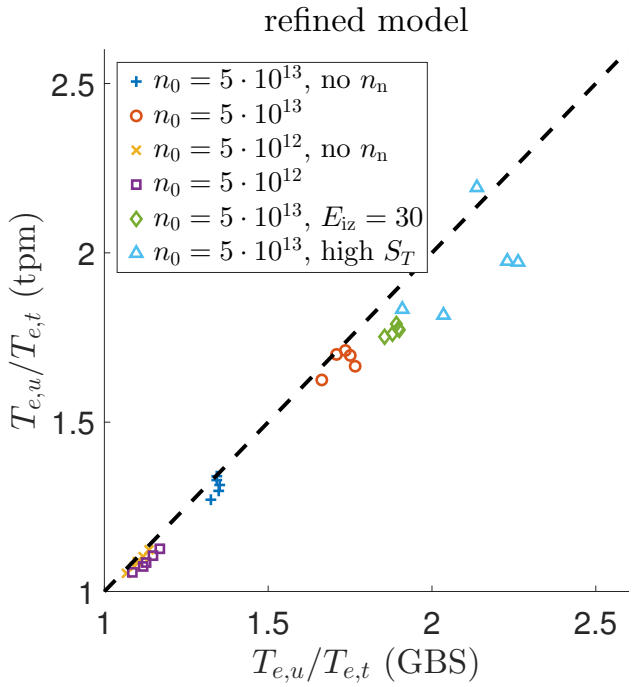

Figure 4: Comparison of the ratio between the electron temperature at the upstream and target locations, $T_{e,u}/T_{e,t}$, as provided by the refined two-point model, Eqs. (17-18), (tpm), with the same set of GBS simulations considered in Fig. 1 and described in Sec. 3.

With these constraints, for a given density source strength, heat source strength, and total amount of ionization in the observed flux tube, the refined two-point model, consisting of Eqs. (17,18,20,22), can be solved self-consistently. We compare its results to the set of simulations described in Sec. 3 in Fig. 4. The results from the refined two-point model and the simulations show very good agreement.

5 Discussion and conclusions

We test separately the main differences between the simple and the refined two-point model to determine the reason behind the significantly better agreement of the latter with the turbulence simulations. We observe that the shape of the source terms $S_{n\perp}$ and $S_{Q\perp}$ (from constant to a cosine poloidal

dependence) does not improve significantly the agreement of the simple two-point model. On the other hand, a significant effect can be observed by including the plasma-neutral interaction terms. This was also observed by Tokar et al. [16], where an improved two-point model is described in which the neutrals are modeled as exponentially decaying from the limiter, similarly to the approach in the present paper, and charge-exchange collisions are taken into account through a diffusive model. To show the impact of the plasma-neutral interaction on the two-point model, we repeat the comparison between simulation results and the simple two-point model, but we include the plasma-neutral interaction terms (we assume a linear velocity profile to obtain the density, which is only needed in S_{n,n_n}). The results, shown in Fig. 5 (left), reveal that, while the trend shown by the simulations is recovered, there is still a significant offset from GBS results, which disappears in the refined model (Fig. 4), where the compressional term, $v_{\parallel \mathrm{e}} \nabla_\parallel (n T_\mathrm{e})$ [Eq. (18)], originating from the plasma compressibility in the Braginskii equations, is included.

To investigate the effect of the compressional term, we repeat the comparison between simulation results and the refined two-point model, but we neglect the plasma-neutral interaction term. The result is shown in Fig. 5 (right). While for the simulations with low density and without neutrals we observe the same level of agreement between turbulence simulation and this two-point model as in the complete refined two-point model (Fig. 4), the same is not true for high density simulations, where the neutral mean free path is short.

From these observations we can draw two conclusions. First, when considering simulations with short neutral mean free path, it is important to account for the plasma-neutral interaction terms, and second, throughout the parameter regime explored in our simulations, the compressional term has to be taken into account for good quantitative agreement. We note that for significantly higher temperatures the impact of the compressional term might be reduced, since the parallel electron heat conductivity, increasing proportional to $T_\mathrm{e}^{5/2}$, might dominate the heat equation. This has to be investigated with future simulations.

We can conclude that, by taking into account these two effects, the refined two-point model that we derived from the drift-reduced Braginskii equations for the limited tokamak SOL predicts accurately the ratio between upstream and target electron temperatures along a flux tube given three input parameters, namely the particle and heat sources due to perpendicular turbulent

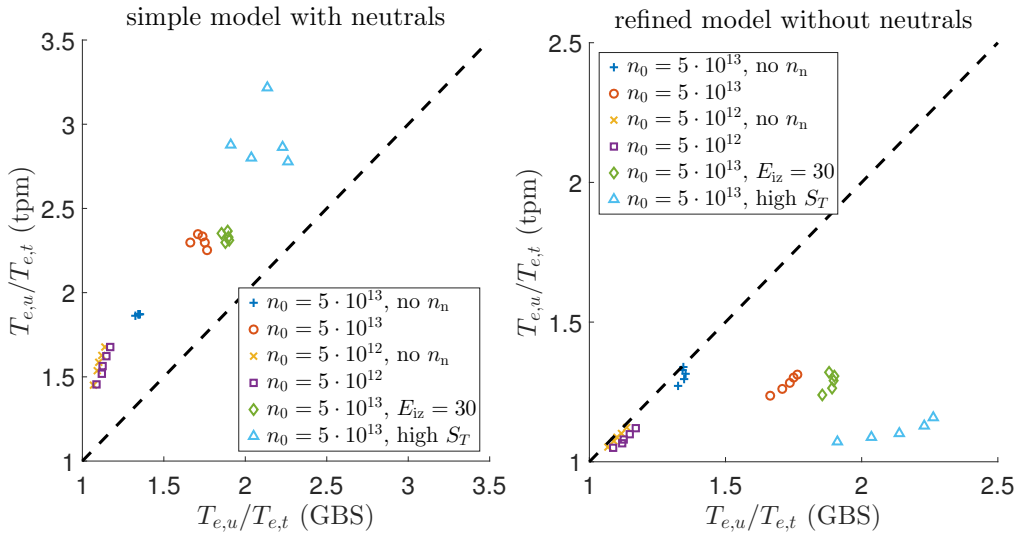

Figure 5: Comparison of the ratio between the electron temperature at the upstream and target locations, $T_{\mathrm{e,u}}/T_{\mathrm{e,t}}$, for two intermediate models between the refined model (Fig. 4) and the simple model (Fig. 1). On the left, results from the the simple two-point model (Sec. 2) are shown, where the plasma-neutral interaction terms have been included to otherwise constant source terms S_n and S_Q. On the right, results from the refined model are shown, where the plasma-neutral interaction terms have been omitted.

transport, and the ionization in the flux tube.

In the present paper, we focus our attention on the electron temperature drop. We would like to remark that evaluating the same drop for the ion temperature brings additional difficulties. In fact, using quasi-neutrality to derive the drift-reduced Braginskii equations, we choose the electron density equation to evolve the plasma density. Therefore, identifying the parallel and perpendicular transport terms in the electron heat equation, Eq. (16), which is a combination of the density and electron temperature equation [Eq. (3) and Eq. (7)], is straightforward. Applying the same procedure to separate the parallel and perpendicular dynamics in an ion heat equation requires the use of the ion density equation, that involves the ion polarization velocity (see, e.g., [18]), which is more challenging. Furthermore, while neglecting the plasma current term in the electron equation is a good assumption (the 'JP' term in Fig. 3 is always smaller than several other dominant terms), we have observed that in the ion temperature balance (not shown) the current term

can dominate the balance at certain locations. In general, it is difficult to estimate the magnitude of the parallel current. Additionally, the complexity of the plasma-neutral interaction increases for the ions due to charge-exchange collisions, whose evaluation needs an approximation of the neutral temperature, while the neutral density suffices for the electron equations. On the other hand, the parallel heat conduction is much smaller for the ions than for the electrons, and can be neglected in most cases.

To conclude, this paper presents, to our knowledge, the first comparison between a two-point model including plasma-neutral interactions and turbulence simulations of the tokamak SOL. This comparison has ultimately allowed us to develop a refined two-point model, which reproduces well the simulation results. It can be used, in the parameter regime investigated with our simulations, to approximately predict the outcome of computationally expensive turbulence simulations, guiding the decision about input parameters of such simulations or experiments. As progress in the development of three-dimensional turbulence codes evolves, we can foresee improvements of two-point models in more advanced tokamak exhaust configurations.

6 Acknowledgments

The authors acknowledge useful discussions with F. Halpern, F. Riva, C. Theiler, and C. Tsui. Part of the simulations presented herein were carried out using the HELIOS supercomputer system at Computational Simulation Centre of International Fusion Energy Research Centre (IFERC-CSC), Aomori, Japan, under the Broader Approach collaboration between Euratom and Japan, implemented by Fusion for Energy and JAEA; and part were carried out at the Swiss National Supercomputing Centre (CSCS) under Project IDs s549 and s655. This research was supported in part by the Swiss National Science Foundation, and has been carried out within the framework of the EUROfusion Consortium and has received funding from the Euratom research and training programme 20142018 under grant agreement No. 633053. The views and opinions expressed herein do not necessarily reflect those of the European Commission.

References

[1] A Loarte, B Lipschultz, A.S Kukushkin, G.F Matthews, P.C Stangeby, N Asakura, G.F Counsell, G Federici, A Kallenbach, K Krieger, A Mahdavi, V Philipps, D Reiter, J Roth, J Strachan, D Whyte, R Doerner, T Eich, W Fundamenski, A Herrmann, M Fenstermacher, P Ghendrih, M Groth, A Kirschner, S Konoshima, B LaBombard, P Lang, A.W Leonard, P Monier-Garbet, R Neu, H Pacher, B Pegourie, R.A Pitts, S Takamura, J Terry, E Tsitrone, the ITPA Scrape-off Layer, and Diver Group. Chapter 4: Power and particle control. Nuclear Fusion, 47(6):S203–S263, jun 2007.

[2] P. Stangeby. The plasma boundary of magnetic fusion devices. IOP Publishing, 2000.

[3] B.D. Dudson, M.V. Umansky, X.Q. Xu, P.B. Snyder, and H.R. Wilson. BOUT++: A framework for parallel plasma fluid simulations. Computer Physics Communications, 180(9):1467–1480, sep 2009.

[4] P. Ricci, F. D. Halpern, S. Jolliet, J. Loizu, A. Mosetto, A. Fasoli, I. Furno, and C. Theiler. Simulation of plasma turbulence in scrape-off layer conditions: the GBS code, simulation results and code validation. Plasma Physics and Controlled Fusion, 54(12):124047, Nov 2012.

[5] F.D. Halpern, P. Ricci, S. Jolliet, J. Loizu, J. Morales, A. Mosetto, F. Musil, F. Riva, T.M. Tran, and C. Wersal. The gbs code for tokamak scrape-off layer simulations. Journal of Computational Physics, 315:388408, Jun 2016.

[6] Andreas Stegmeir, David Coster, Omar Maj, Klaus Hallatschek, and Karl Lackner. The field line map approach for simulations of magnetically confined plasmas. Computer Physics Communications, 198:139–153, jan 2016.

[7] P. Tamain, H. Bufferand, G. Ciraolo, C. Colin, D. Galassi, Ph. Ghendrih, F. Schwander, and E. Serre. The TOKAM3x code for edge turbulence fluid simulations of tokamak plasmas in versatile magnetic geometries. Journal of Computational Physics, 321:606–623, sep 2016.

[8] H. Bufferand, B. Bensiali, J. Bucalossi, G. Ciraolo, P. Genesio, Ph. Ghendrih, Y. Marandet, A. Paredes, F. Schwander, E. Serre, et al. Near wall plasma simulation using penalization technique with the transport code SOLEDGE2D-EIRENE. Journal of Nuclear Materials, 438:S445–S448, 2013.

[9] D. Reiter. Progress in two-dimensional plasma edge modelling. Journal of Nuclear Materials, 196-198:8089, Dec 1992.

[10] R. Schneider, D. Reiter, H. P. Zehrfeld, B. Braams, M. Baelmans, J. Geiger, H. Kastelewicz, J. Neuhauser, and R. Wunderlich. B2-EIRENE simulation of ASDEX and ASDEX-upgrade scrape-off layer plasmas. Journal of Nuclear Materials, 196-198:810815, Dec 1992.

[11] D. Reiter, M. Baelmans, and P. Börner. The EIRENE and B2-EIRENE codes. Fusion Science and Technology, 47(2):172–186, 2005.

[12] Y. Feng, F. Sardei, J. Kisslinger, P. Grigull, K. McCormick, and D. Reiter. 3D edge modeling and island divertor physics. Contributions to Plasma Physics, 44(13):5769, Apr 2004.

[13] T. D. Rognlien, J. L. Milovich, M. E. Rensink, and G. D. Porter. A fully implicit, time dependent 2-D fluid code for modeling tokamak edge plasmas. Journal of Nuclear Materials, 196-198:347351, Dec 1992.

[14] Y. Marandet, A. Mekkaoui, D. Reiter, P. Boerner, P. Genesio, F. Catoire, J. Rosato, H. Capes, L. Godbert-Mouret, M. Koubiti, and et al. Transport of neutral particles in turbulent scrape-off layer plasmas. Nuclear Fusion, 51(8):083035, Jul 2011.

[15] P C Stangeby. A tutorial on some basic aspects of divertor physics. Plasma Phys. Control. Fusion, 42(12B):B271–B291, dec 2000.

[16] M. Z. Tokar, M. Kobayashi, and Y. Feng. Improved two-point model for limiter scrape-off layer. Phys. Plasmas, 11(10):4610, 2004.

[17] V Kotov and D Reiter. Two-point analysis of the numerical modelling of detached divertor plasmas. Plasma Phys. Control. Fusion, 51(11):115002, oct 2009.

[18] A. Zeiler, J. F. Drake, and B. Rogers. Nonlinear reduced Braginskii equations with ion thermal dynamics in toroidal plasma. Phys. Plasmas, 4(6):2134, 1997.

[19] C. Wersal and P. Ricci. A first-principles self-consistent model of plasma turbulence and kinetic neutral dynamics in the tokamak scrape-off layer. Nuclear Fusion, 55(12):123014, Nov 2015.

[20] S. I. Braginskii. Transport processes in a plasma. Reviews of Plasma Physics, 1:205, 1965.

[21] J. Loizu, P. Ricci, F. D. Halpern, and S. Jolliet. Boundary conditions for plasma fluid models at the magnetic presheath entrance. Phys. Plasmas, 19(12):122307, 2012.

[22] Akio Arakawa. Computational design for long-term numerical integration of the equations of fluid motion: Two-dimensional incompressible flow. part i. Journal of Computational Physics, 1(1):119–143, aug 1966.

[23] Martin Wilhelm Kutta. Beitrag zur näherungsweisen Integration totaler Differentialgleichungen. Zeitschrift für Mathematik und Physik, 46:435–453, 1901.